

# Predicting Uniaxial Cyclic Compressive Behavior of Brick Masonry: New Analytical Model

Luca Facconi<sup>1</sup>; Fausto Minelli<sup>2</sup>; and Frank J. Vecchio, M.ASCE<sup>3</sup>

**Abstract:** A constitutive model for simulating the compressive response of unreinforced brick masonry subjected to cyclic loading is presented and discussed. The developed formulations are consistent with the smeared rotating crack approach and may be easily implemented in finite element codes for nonlinear analysis. The analysis approach includes different features such as nonlinear curves for capturing the shape of the unloading/reloading branches, both in case of full unloading from the envelope curve and partial unloading/reloading. A unified model for predicting the residual plastic strain as a function of the strain recovered during unloading is also proposed. Particular attention is paid to the stiffness degradation occurring during reloading and to the prediction of the stress and strain values at which the reloading branch intersects the envelope. The calibration of most of the proposed formulations is based on experimental results reported in the literature, as well as from two uniaxial cyclic compression tests carried out within the present work. Finally, the model effectiveness is tested with some verification examples. DOI: 10.1061/(ASCE)ST.1943-541X.0001961. © 2017 American Society of Civil Engineers.

**Author keywords:** Masonry; Nonlinear analysis; Cyclic loading; Compressive behavior; Residual plastic strain; Constitutive model.

## Introduction

In the last decades, the use of numerical nonlinear simulations for predicting the response of masonry structures has become quite common among engineers because of the increasing computational power and processing capability of electronic devices. The analysis methods generally implemented are based on two main approaches named micromodeling and macromodeling. The former (Lourenço and Rots 1997; Mehrabi and Shing 1997; Chaiyoon and Attard 2007) consists of separately modeling the masonry components and considering the failure mechanisms that characterize joints and units. The latter (Gambartotta and Lagomarsino 1997; Lourenço et al. 1998; Vecchio 2000; Papa 2001; Facconi et al. 2014) considers masonry as a continuum where the material properties are smeared over a finite region of the structure in which stresses are sufficiently uniform and a relation between the average stresses and strains is established. Micromodeling provides a detailed description of local behavior of masonry, but its high computational cost makes this approach suitable for relatively small elements. On the contrary, when the analysis of the entire structure response is more important than the behavior of single structural elements, macromodeling appears to be more convenient, leading to a good compromise between analysis accuracy and computation time (Rots 1988).

Macromodels require the implementation of constitutive stress-strain laws that are able to represent the uniaxial compressive

response of masonry. In regards to masonry subjected to cyclic loading, the literature reports a limited number of constitutive models which cannot be easily generalized for the prediction of the masonry cyclic compressive response. Subramaniam and Sinha (1995) proposed analytical formulations for modeling the unloading and reloading curves of brick masonry loaded both perpendicularly and parallel to bed joints. This model represents an important reference because its calibration is based on a significant amount of experimental data resulting from tests on clay brick masonry panels (Naraine and Sinha 1989b). In spite of this fact, the applicability of the model cannot be unconditionally extended to any type of masonry material. Eibl et al. (1996) formulated a model in which the unloading curve is represented by an exponential relationship, whereas the reloading path is approximated with a linear curve. The model can be easily implemented, but the basic points used to determine the unloading and the reloading curve are defined according to the test results reported by Naraine and Sinha (1989a). Moreover, when formulating the model, the authors make no mention of the model behavior in case of partial unloading-reloading. The more refined model proposed by Crisafulli (1997) is able to provide a comprehensive description of the nonlinear path typically followed by the unloading and the reloading curves. Unlike other models, the Crisafulli model considers the case of partial unloading-reloading as well as the response in case of accumulative damage due to small cycle hysteresis. However, in order to get a prediction of the cyclic response, the nine empirical coefficients used in the model equations have to be initially calibrated and defined by considering the related ranges of variation suggested by the author. More recently, Sima et al. (2011) proposed a constitutive model whose material parameters are obtained from the linear regression of the experimental data reported by Naraine and Sinha (1989a). As in other models, the constitutive law assumes a nonlinear unloading curve followed by a simple linear reloading response. The model includes a rule for modeling the general case of partial unloading-reloading, but the authors do not provide a specific calibration of the model parameters because of the lack of experimental information provided by literature.

Although the study of the dynamic behavior of masonry structures has become ever more important for many application fields, for example, in seismic engineering, a limited number of

<sup>1</sup>Postdoctoral Fellow, Dept. of Civil, Environmental, Architectural Engineering and Mathematics, Univ. of Brescia, Via Branze, 43, 25123 Brescia, Italy (corresponding author). E-mail: luca.facconi@unibs.it; lucafacconi@hotmail.com

<sup>2</sup>Associate Professor, Dept. of Civil, Environmental, Architectural Engineering and Mathematics, Univ. of Brescia, Via Branze, 43, 25123 Brescia, Italy.

<sup>3</sup>Professor, Dept. of Civil Engineering, Univ. of Toronto, Toronto, ON, Canada M5S 1A4.

Note. This manuscript was submitted on February 22, 2017; approved on August 9, 2017; published online on December 14, 2017. Discussion period open until May 14, 2018; separate discussions must be submitted for individual papers. This paper is part of the *Journal of Structural Engineering*, © ASCE, ISSN 0733-9445.

experimental studies on the cyclic compressive behavior of brick masonry are available. The first detailed investigation was performed by Naraine and Sinha (1989a, b), who tested 18 clay brick masonry specimens loaded both perpendicularly and parallel to mortar bed joints. The same authors (Naraine and Sinha 1991a) also performed tests on half-scale clay brick panels subjected to biaxial cyclic loading. The mean compressive strength of bricks and mortar used by Naraine and Sinha to construct the test samples were respectively equal to approximately 13.4 and 6.4 MPa. Later, AlShebani and Sinha (1999) carried out uniaxial tests on masonry panels made of sand-plast half brick units having a mean compressive strength of 23.4 MPa, and mortar with a mean compressive strength of 10.2 MPa. Again, the tests were conducted by loading specimens parallel and normally to bed joints. All the previous studies focused on the determination of the stability point and the common point curves as well as the residual plastic strains that characterize the compression cyclic response of masonry. Oliveira (2003) performed cyclic tests on small stacked bond prisms made with solid clay bricks (mean mortar compressive strength = 5.5 MPa) in order to get information on brittleness, energy dissipation, and stiffness degradation. More recently, Galman (2012) performed tests on specimens made of solid clay bricks and mortar having a compressive strength of 18.7 and 6.8 MPa, respectively. The research included single- and double-wythe brick panels loaded perpendicularly to bed joints. Unlike all the previous researches, Ispir and Ilki (2013) investigated the compressive cyclic behavior of existent solid brick masonry by testing 15 panels extracted from different walls of historical houses. As typical for historical materials, the bricks and mortar presented quite low mean compressive strengths equal to 5.5 and 3.1 MPa, respectively.

This paper aims to propose an analytical model for predicting the cyclic compressive response of brick masonry. In view of its implementation in the disturbed stress field model (DSFM) for unreinforced masonry (Faconi et al. 2014), the model is formulated in the context of the smeared rotating crack approach. In order to obtain a realistic representation of the actual material behavior, both the reloading and the unloading curves have been modeled using suitable nonlinear curves. The calibration of the main model parameters has been based on experimental data concerning different brick masonry typologies. Partial unloading and reloading has also been included to better capture the possible loading histories occurring during seismic events. As proved by the verification examples reported at the end of the paper, a reasonable prediction of the masonry behavior can be obtained by implementing the proposed model with the suggested default values of the basic parameters. Therefore, the model may be a useful tool for easily obtaining a preliminary prediction of the compressive behavior without performing experimental tests for its calibration. It is also noteworthy that the model has been calibrated on the results of quasi-static cyclic tests and, moreover, its formulations cannot be extended to the analysis of materials subjected to a high number of load repetitions (fatigue analysis).

The model formulation is preceded by the presentation of the results obtained from two uniaxial compression cyclic tests on solid clay brick panels carried out at the University of Brescia. The data provided by the test results have been used for the model calibration together with those collected from the literature.

## Cyclic Compression Tests on Masonry Panels

### Test Specimen

Two masonry prisms with dimensions  $780 \times 510 \times 245$  mm<sup>3</sup> were built with solid clay brick units measuring  $250 \times 120 \times 60$  mm<sup>3</sup>.

The compression tests performed according to BS EN 772-1: 2011 (BSI 2011) on six brick specimens provided a normalized mean compressive strength equal to 12.5 MPa [coefficient of variation (COV) = 9%]. Bricks were laid on a running bond by using alternated stretchers and headers, with the headers of each row centered on the stretchers of the row below. All samples contained 11 courses of bricks with a nominal mortar head and bed joint thickness of 10 mm. The latter was prepared using a commercial ready-mix mortar containing hydraulic lime, portland cement, and sand. A total of 15 mortar prismatic specimens having dimensions  $160 \times 40 \times 40$  mm<sup>3</sup> were tested according BS EN 1015-11 (BSI 2007) after more than 28 days from casting. The resulting mean cube compressive and flexural strength were equal to 7.7 MPa (COV = 10%) and 2.4 MPa (COV = 13%), respectively.

Before constructing the masonry panels, the clay bricks were soaked in water for approximately 1 h until complete saturation. To maintain uniform workmanship, the same mason built all the samples. After construction, each specimen was cured for 28 days by keeping it wet and covered with a polyethylene sheet. Two samples, named respectively MPC1 and MPC2, were tested 55 days after construction.

### Test Set-Up and Instrumentation

The specimens were tested under uniaxial loading by means of the test arrangement depicted in Fig. 1. The masonry panel was placed between a load distributor beam and a RC slab laid on the laboratory strong floor immediately after leveling by a thin mortar layer. A 6-mm-thick steel plate was fixed both at the top and at the bottom of the specimen. The loading rig consisted of a steel reaction frame anchored to the bottom surface of the strong floor and connected to an electromechanical jack having a capacity of 1,000 kN. A steel beam (2UPN400) hinged to the actuator allowed the transfer of load to two Dywidag bars (Dywidag S.p.A., Cusago, Milan, Italy) passing through the floor and bolted to the loading beam. A steel roller was positioned between the loading and the distributor beam to concentrate the force along the vertical axis of the specimen. The applied load was monitored by two load cells placed on the loading beam and connected to the Dywidag bars.

Potentiometric transducers were used to measure axial and lateral displacements on both sides of the specimen (Fig. 2). More specifically, transducers VS1–VS2 and VS3–VS4 measured the vertical deformations, whereas transducers HS1 and HS2 detected the horizontal deformations. The gauge length was kept constant at 420 mm, for the axial deformation transducers, and 300 mm for the lateral deformation transducers.

The two specimens were tested under cyclic loading at a constant displacement rate of 0.01 mm/s in the loading and reloading stage, and 0.05 mm/s in the unloading stage. An incremental strain of approximately  $0.1 \times 10^{-3}$  in each cycle was generally adopted to allow the loading curve to attain the envelope curve. The electronic speed control device of the thrust jack was unable to provide stable control of the test once the peak load was achieved. Therefore, it was not possible to detect the postpeak response of either specimens.

### Experimental Test Results

The compressive axial stress-strain curves obtained from the cyclic tests are depicted in Fig. 3. The peak strengths ( $f_{m,p}$ ) exhibited by specimens MPC1 and MPC2 were equal to 8.22 and 7.77 MPa, respectively. The strain detected at peak strength ( $\epsilon_p$ ) was 1.59 mm/m for specimen MPC1 and 3.15 mm/m for specimen MPC2. Despite the two panels having similar geometrical and

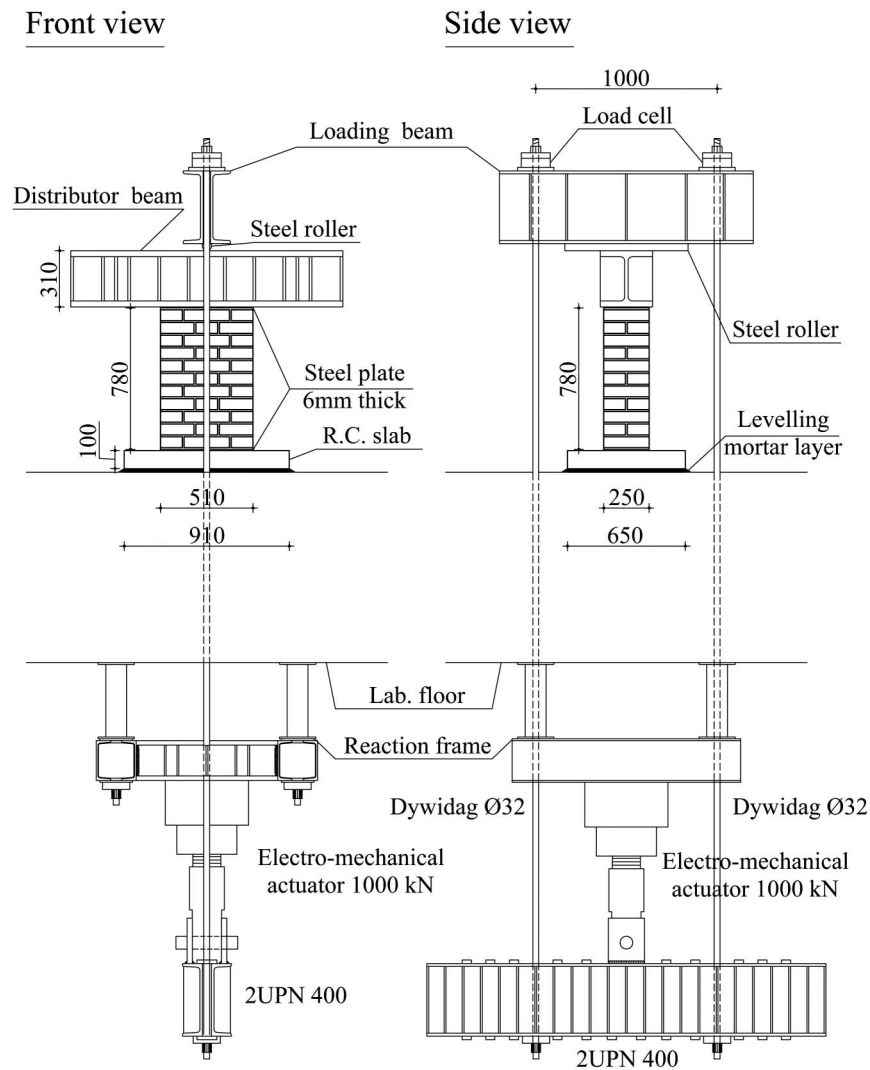


Fig. 1. Loading set-up (dimensions in millimeters)

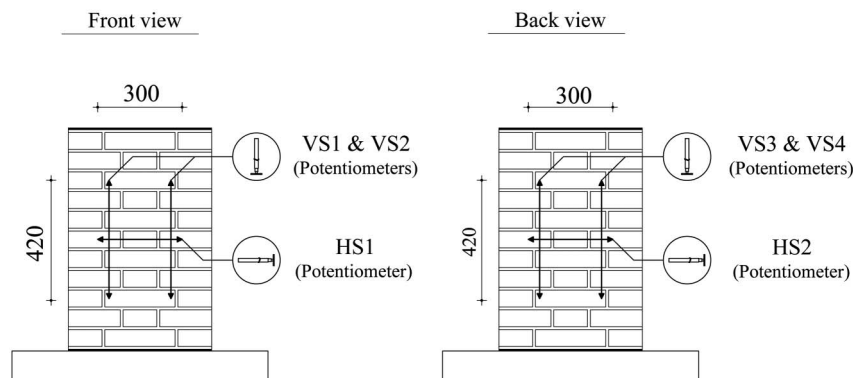


Fig. 2. Schematic of the instrumentation (dimensions in millimeters)

material properties, the response of specimen MPC1 appeared to be stiffer than that exhibited by MPC2. In fact, the strain  $\varepsilon_p$  of the former was 50% lower than that exhibited by the latter. On the contrary, the peak strength of specimen MPC1 was only 6% higher than that of specimen MPC2.

The crack patterns of the two samples, observed at the end of the test, presented similar features. As shown in Fig. 4, splitting cracks due to the tensile failure of bricks occurred on both short sides of

the sample [Figs. 4(c and d)], whereas tensile cracks parallel to the axial load were detected on the front and back side on bricks as well as bed joints [Figs. 4(a and b)].

Seismic performance is frequently represented by the dissipated energy. The energy density dissipated within each cycle ( $E$ ), that is, the area enclosed in the unloading-reloading cycle of the stress-strain curve, is represented in Fig. 5 as a function of the normalized strain at peak stress of each cycle ( $\varepsilon'_p$ ), that is, the ratio between

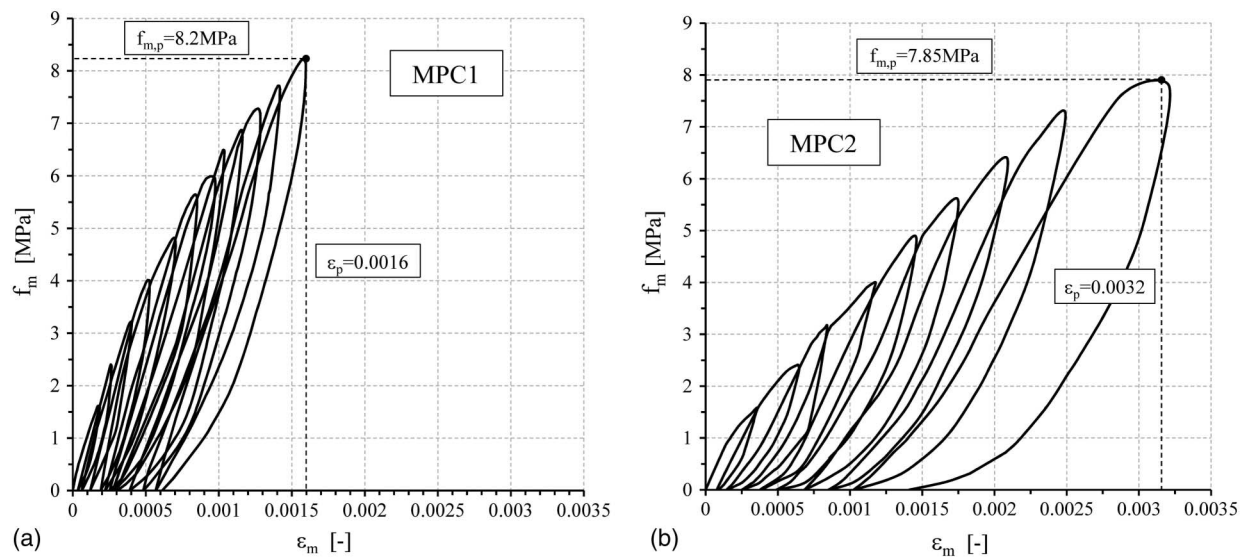


**Fig. 3.** Compression stress ( $f_m$ )-strain ( $\epsilon_m$ ) curves obtained from the cyclic tests on (a) specimen MPC1; (b) specimen MPC2

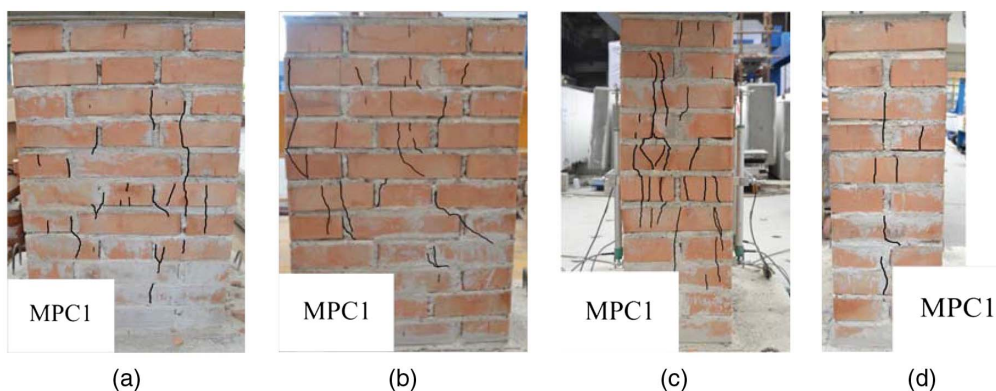


**Fig. 4.** Typical crack pattern at peak load: (a) front side; (b) back side; (c) and (d) short-side view

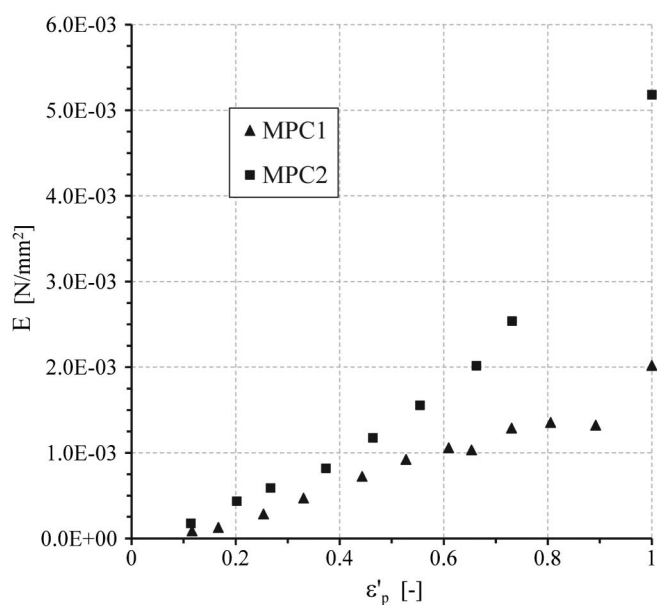


**Fig. 5.** Dissipated energy density ( $E$ ) versus normalized strain at peak strength of each cycle ( $\epsilon'_p$ )

strain at peak stress of each cycle and the strain at peak strength of the overall response ( $\epsilon_p$ ). Fig. 5 highlights the progressive increment of the dissipated energy for increasing values of  $\epsilon'_p$ . Moreover, because of its higher deformability, the total energy dissipated by specimen MPC2 was approximately 2.2 times higher than that dissipated by specimen MPC1.

Compared with the specimen MPC2, the specimen MPC1 exhibited a higher compressive stiffness and a lower dissipated energy density. These results can be explained considering the damage pattern presented by the samples at the end of the test. In spite of their similar crack patterns, specimen MPC2 developed a higher number of cracks that led to a reduced stiffness, as well as to a higher fracture surface and, therefore, energy. Moreover, the axial stiffness of specimen MPC2 was affected, especially in the initial stage of the test, by existing cracks due to both material imperfections and mortar shrinkage.

### Model Formulation

The study herein reported is part of a broader research program aimed to propose an improvement of the DSFM for unreinforced masonry (DSFM-UM) (Faconi et al. 2014) that allows simulating the reverse cyclic behavior of masonry structures. Thus, the model

has been formulated in the context of smeared rotating cracks, and is intended to be implemented within the existing formulations. The comprehensive model, including constitutive laws representing the cyclic behavior of masonry in tension, will be presented in a future work together with the results of some nonlinear finite element simulations of masonry structures under cyclic loading.

### Envelope Curve

As shown by Naraine and Sinha (1989b), the envelope curve for masonry subjected to axial cyclic compressive load can be reasonably represented by the monotonic stress-strain curve. The monotonic relationship adopted here is subdivided into a prepeak and a postpeak curve, which represent the compressive behavior before and after the attainment of the peak strain  $\varepsilon_p$ . For the prepeak curve, the model proposed by Hoshikuma et al. (1997) for concrete allows the input of the initial elastic modulus of masonry. The postpeak response is modeled by a simple parabolic curve that generally provides a suitable representation of the strength degradation occurring for most masonry typologies. Thus, the overall envelope curve may be described as

$$\begin{aligned} f_m &= E_m \cdot \varepsilon_m \cdot \left[ 1 - \frac{1}{n} \left( \frac{\varepsilon_m}{\varepsilon_p} \right)^{n-1} \right] & \text{for } \varepsilon_m \leq \varepsilon_p \\ f_m &= f_{m,p} \cdot \left[ 1 - \left( \frac{\varepsilon_m - \varepsilon_p}{\varepsilon_u - \varepsilon_p} \right)^2 \right] & \text{for } \varepsilon_m > \varepsilon_p \end{aligned} \quad (1)$$

where  $f_m$  and  $\varepsilon_m$  = stress and the strain acting in the masonry, respectively;  $\varepsilon_p$  and  $f_{m,p}$  = strain at the peak and the corresponding strength; and  $\varepsilon_u$  = ultimate strain at zero stress. The latter is not generally easy to evaluate because experimental tests are often interrupted before reaching the complete distress of the specimen. Tests carried out by different researchers have shown that  $\varepsilon_u$  can assume values even higher than 1.5–2 times  $\varepsilon_p$ . The parameter  $n = E_m / (E_m - E_{sec})$  is a function of both the initial elastic tangent modulus  $E_m$  and the secant modulus  $E_{sec} = f_{m,p} / |\varepsilon_p|$ . The envelope curve adopted here is consistent with that used in the DSFM-UM to represent the monotonic compressive stress-strain behavior of masonry. However, the formulation of the cyclic model described subsequently can be easily adapted to different envelope curve typologies equally able to represent the compressive behavior of masonry.

Fig. 6 compares the cyclic stress-strain curves of specimen MPC1, MPC2, and of some experimental tests reported in the literature (Naraine and Sinha 1989a; Galman 2012; Oliveira 2003), with the related envelope curves based on Eq. (1). The parameters implemented in the analytical model to fit the experimental data are summarized in Table 1. It appears that the proposed model is generally able to provide a good representation of the experimental data in both the prepeak and in the postpeak responses. Except for the test carried out by Naraine and Sinha (1989a), the envelope curves tend to exhibit a strength overestimation that will necessarily affect the accuracy of the cyclic response predicted by the model. This fact is shown by the simulation results reported in the “Model Verification” section of the paper.

### Plastic Offset Model

The plastic offset strain,  $\varepsilon_{pl}$  (i.e., the residual strain at the end of unloading at zero-load level), represents the amount of irrecoverable damage of composite material resulting from the loading and unloading process. Therefore,  $\varepsilon_{pl}$  is a fundamental parameter for determining the shape of the unloading path and for estimating the degree of damage occurring in masonry during cycling.

The literature provides few models specifically developed for predicting the plastic offset strain for brick masonry. Based on the results of different experimental programs on brick masonry, Naraine and Sinha (1989b), Subramaniam and Sinha (1995), and AlShebani (2001) proposed empirical equations that allow the calculation of  $\varepsilon_{pl}$  for loading perpendicular and parallel to bed joints. The experimental results reported by those authors and by other researchers (Galman 2012; Ispir and Ilki 2013), as well as the plastic strains obtained from the two tests discussed previously in this paper, have been here used for proposing a comprehensive and more general formulation to predict the residual strain. The proposed model aims at reducing the dependency on a single set of experimental data and tests conditions that affect the aforementioned empirical models reported in the literature. Fig. 7 reports the values of the normalized plastic strain ( $\varepsilon'_{pl} = \varepsilon_{pl} / \varepsilon_p$ ) and the corresponding normalized unloading strain ( $\varepsilon'_{un}$ ) (i.e., the normalized strain detected on the unloading-reloading curve where it intercepts the envelope curve) in comparison with the proposed analytical model. The latter consists of the following parabolic equation:

$$\varepsilon'_{pl} = 0.235 \cdot (\varepsilon'_{un})^2 + 0.25 \cdot |\varepsilon'_{un}| \quad (2)$$

which provides a best fit to the experimental data. A similar equation was proposed by Palermo and Vecchio (2003) for reinforced concrete.

The proposed formulation represents a unified model derived from uniaxial and biaxial tests carried out by loading specimens both perpendicularly and parallel to bed joints. This assumption is supported by the outcomes of the studies performed by Naraine and Sinha (1989a, 1991a), who highlighted the reduced influence of the loading direction on the residual plastic strains. Thus, Eq. (2) is supposed to be suitable for evaluating the plastic strain irrespective of the loading direction and the ratio between principal stresses.

### Unloading-Reloading Model

#### Unloading Curve

As pointed out by Naraine and Sinha (1989b), the curve representing the behavior of masonry in the unloading stage is typically nonlinear, and its shape depends on the strain level ( $\varepsilon_{un}$ ) at which unloading occurs. The unloading branch is represented by the analytical model proposed by Crisafulli (1997), the general formulation of which is given as follows:

$$f_m = f_1 + (f_2 - f_1) \cdot \frac{B_1 \cdot \chi + \chi^2}{1 + B_2 \cdot \chi + B_3 \cdot \chi^2} \quad (3)$$

where  $f_1$  and  $f_2$  are, respectively, the stresses defining the initial and final point of the curve and  $\chi = (\varepsilon_m - \varepsilon_{un}) / (\varepsilon_{pl} - \varepsilon_{un})$ . For the unloading curve, the initial stress  $f_1$  is assumed equal to the stress ( $f_{m,un}$ ) and the strain ( $\varepsilon_{un}$ ) at onset of unloading, whereas the stress  $f_2$  can be equal to 0, in the case of full unloading from the envelope curve (Fig. 8), or to  $f_{m,ro}$  in the case of partial unloading [Fig. 9(b)]. A typical representation of the unloading curve is depicted in Fig. 8.

Three equations are used to determine the coefficients  $B_1$ ,  $B_2$ , and  $B_3$ :

$$B_1 = \frac{E_1}{E_s}; \quad B_2 = B_1 - B_3; \quad B_3 = 2 - \frac{E_2}{E_s} (1 + B_1) \quad (4)$$

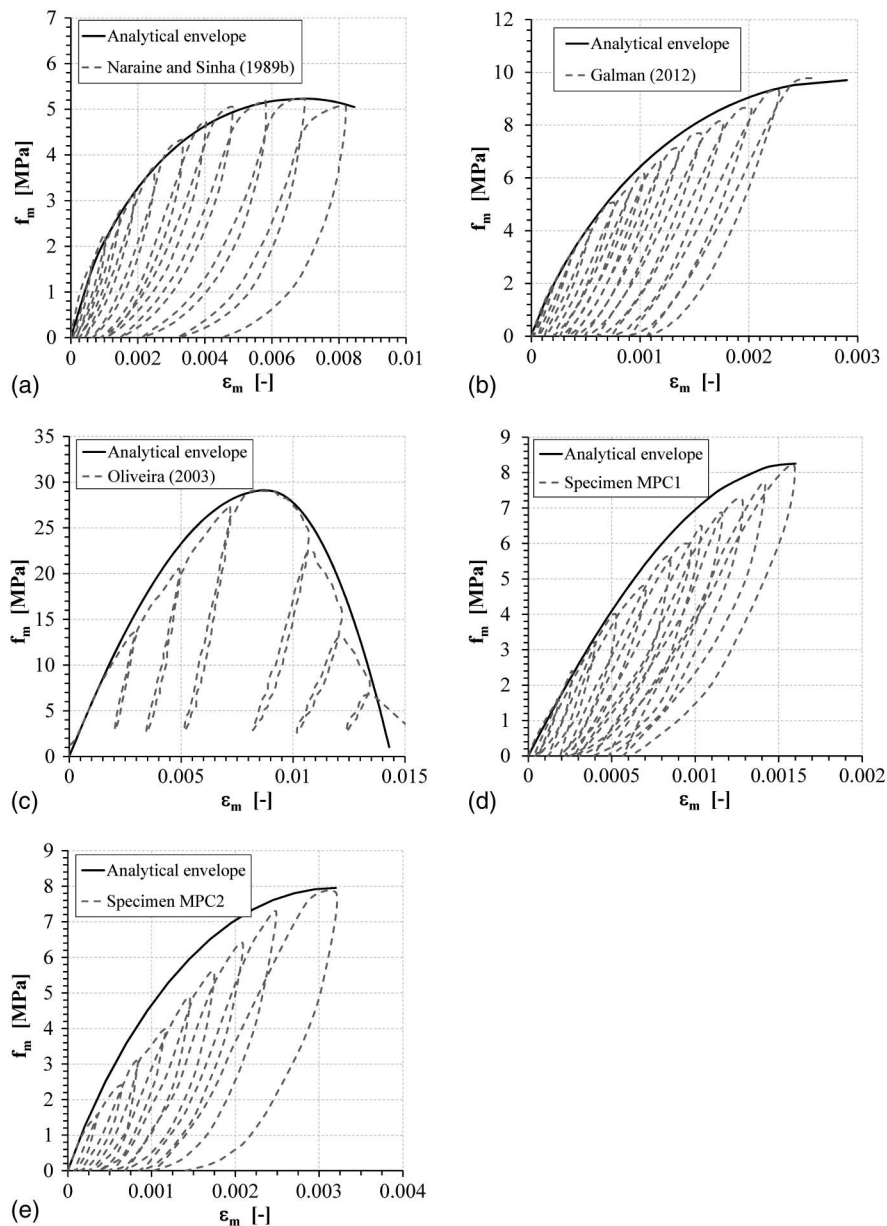


**Fig. 6.** Comparison of the proposed envelope curve with the experimental hysteretic response: (a) Naraine and Sinha (1989b); (b) Galman (2012); (c) Oliveira (2003); (d) Specimen MPC1; (e) Specimen MPC2

**Table 1.** Model Input Data Used in the Verification Case Studies

Case study	Masonry type	$E_m$ (MPa)	$f_{m,p}$ (MPa)	$\varepsilon_p$ (%)	$\varepsilon_u$ (%)
Naraine and Sinha (1989b)	Double wythe frogged clay bricks	9,000	5.23	6.96	15.00
Oliveira (2003)	Single wythe solid clay bricks	6,000	29.10	8.80	14.40
Galman (2012)	Double wythe solid clay bricks	15,000	9.70	2.90	—
Specimen MPC1	Double wythe solid clay bricks	8,800	8.25	1.60	—
Specimen MPC2	Double wythe solid clay bricks	7,400	7.95	3.20	—

where  $E_s = f_{m,un}/(\varepsilon_{un} - \varepsilon_{pl})$  is the secant modulus calculated between the points  $(f_{m,un}, \varepsilon_{un})$  and  $(0, \varepsilon_{pl})$ , whereas  $E_1 = E_{un}$  and  $E_2 = E_{un,pl}$  are the initial and the final tangent moduli. The latter can be evaluated as follows:

$$E_{un} = \gamma_{un} \cdot E_m; \quad E_{un,pl} = \frac{\gamma_{pl,u} \cdot E_m}{\left(1 + \frac{\varepsilon_{un}}{\varepsilon_p}\right)^e} \quad (5)$$

The empirical coefficients  $\gamma_{un} = 1.5$ ,  $\gamma_{pl,u} = 0.15$ , and  $e = 2$  have been determined from best fitting of the unloading curves reported in the literature. Despite the parameter calibration performed, some experimental results have shown that the proposed coefficient  $\gamma_{un}$  could require an adjustment to better fit the experimental response. In case such a modification is required, the value of  $\gamma_{un}$  should be chosen in the range 1.5–3.

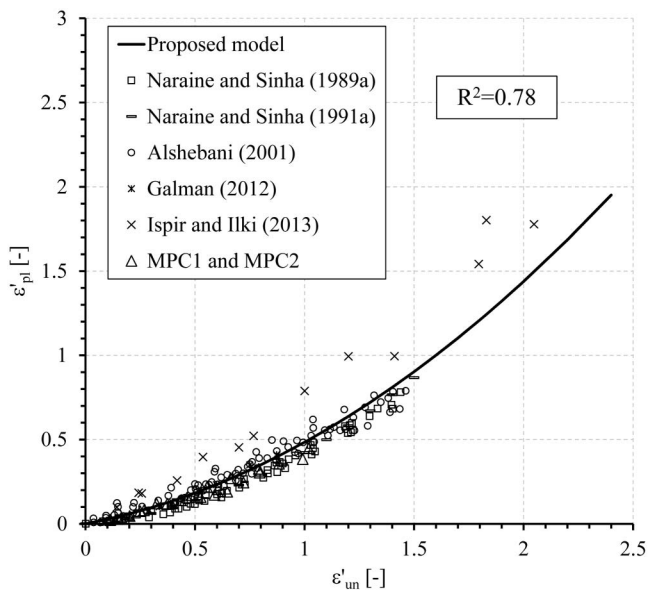


**Fig. 7.** Normalized plastic strain ( $\varepsilon'_{pl}$ ) versus normalized unloading strain ( $\varepsilon'_{un}$ )

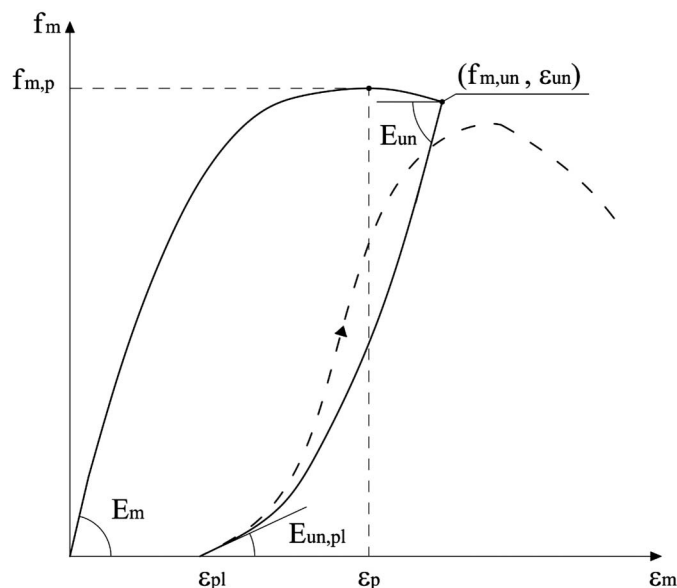


**Fig. 8.** Typical stress-strain unloading curve

The slope of the initial ( $E_{un}$ ) and final ( $E_{un,pl}$ ) tangent to the unloading curve, which are considered positive as shown in Fig. 8, are representative of the response generally exhibited by most brick masonry tests. However, some studies have shown that the value of  $E_{un}$  may sometimes be negative because of creep and relaxation phenomena occurring at the beginning of the reverse loading phase. This effect, which is typical of quasi-static tests, is not expected to occur when the structure is subjected to actual cyclic actions, for example, earthquake or wind, and, therefore, it can be neglected without significantly affecting the model accuracy.

### Full Reloading Curve

The reloading stage begins when the compressive strain starts to increase after complete or partial unloading. It is a well-known fact that the reloading curve generally intersects the envelope curve at a strain higher than that attained at the beginning of the unloading

phase ( $\varepsilon_{un}$ ). This phenomenon is due to damage occurring in the masonry because of the cyclic process. Different approaches can be found in the literature for modeling this progressive damage of the material. Seckin (1981) and Mander et al. (1988) proposed models for concrete that define the reloading strain ( $\varepsilon_{re}$ ), that is, the intersection point between the envelope and the reloading curve, and then adjust the reloading branch in order to intersect the envelope curve at this point. In more detail, the model proposed by Seckin allows determining the reloading branch by defining the reloading stiffness as a function of the unloading strain. On the contrary, the approach of Mander et al. (1988) defines a new stress point on the reloading curve that is a function of the previous unloading stress and of the stress at reloading reversal. A nonlinear function is then used to connect the reloading path to the envelope curve at an arbitrary value of the reloading strain. Both Naraine and Sinha (1991a) and Eibl et al. (1996) suggested models specifically developed for unreinforced masonry. The former determines the reloading curve and the reloading strain by using a series of focal points resulting from geometrical considerations of the properties of the experimental curves. The latter formulated a model in which the reloading branch is linear and its intersection with the envelope curve is assumed to be a function of the stress and strain at compression failure of masonry. Crisafulli (1997) assumed the reloading strain to be proportional to the difference between the unloading and plastic strains by means of a linear function depending on an empirical coefficient that has to be experimentally calibrated. The reloading stiffness is then calculated as the unloading stress to reloading strain ratio.

The approach adopted herein to determine the reloading stress and strain is based on the model proposed by Palermo and Vecchio (2003). As shown in Fig. 9, the reloading strain turns out from the intersection of the envelope curve with the following linear relationship:

$$f_{m,re} = f_{m,ro} + E_{re} \cdot (\varepsilon_{re} - \varepsilon_{ro}) \quad (6)$$

where  $E_{re}$  = reloading stiffness;  $f_{m,re}$  and  $\varepsilon_{re}$  = reloading stress and strain, respectively, resulting from the intersection of Eq. (6) with the envelope curve [Eq. (1)]. Note that  $f_{m,ro}$  and  $\varepsilon_{ro}$  correspond to the stress and strain at reloading reversal (partial unloading-reloading response).

The reloading stiffness is provided by the following degrading function:

$$E_{re} = \frac{\beta_d \cdot f_{m,un} - f_{m,ro}}{\varepsilon_{un} - \varepsilon_{ro}} \quad (7)$$

dependent on the damage factor  $\beta_d$ , whose value is given by the following functions:

$$\beta_d = \frac{1}{1 + 0.20 \cdot \varepsilon_{rec}^{0.5}} \quad \text{for } |\varepsilon_m| < |\varepsilon_p| \quad (8)$$

$$\beta_d = \frac{1}{1 + 0.45 \cdot \varepsilon_{rec}^{0.2}} \quad \text{for } |\varepsilon_m| \geq |\varepsilon_p| \quad (9)$$

where  $\varepsilon'_{rec} = (\varepsilon_{un} - \varepsilon_{ro}) / \varepsilon_p$  is the normalized recovery strain (Fig. 9). When total unloading occurs [Fig. 9(a)]  $\varepsilon_{ro} = \varepsilon_{pl}$ . The curves represented by Eqs. (8) and (9) are plotted in the damage factor ( $\beta_d$ )—normalized recovery strain ( $\varepsilon'_{rec}$ ) plots of Fig. 10. Note that the proposed equations are compared with the damage factor values calculated by considering a series of experimental results including the cyclic tests (i.e., specimens MPC1 and MPC2) carried out in the present research. A total of 74 and 20 datum points have been collected for the prepeak and the postpeak stages, respectively.

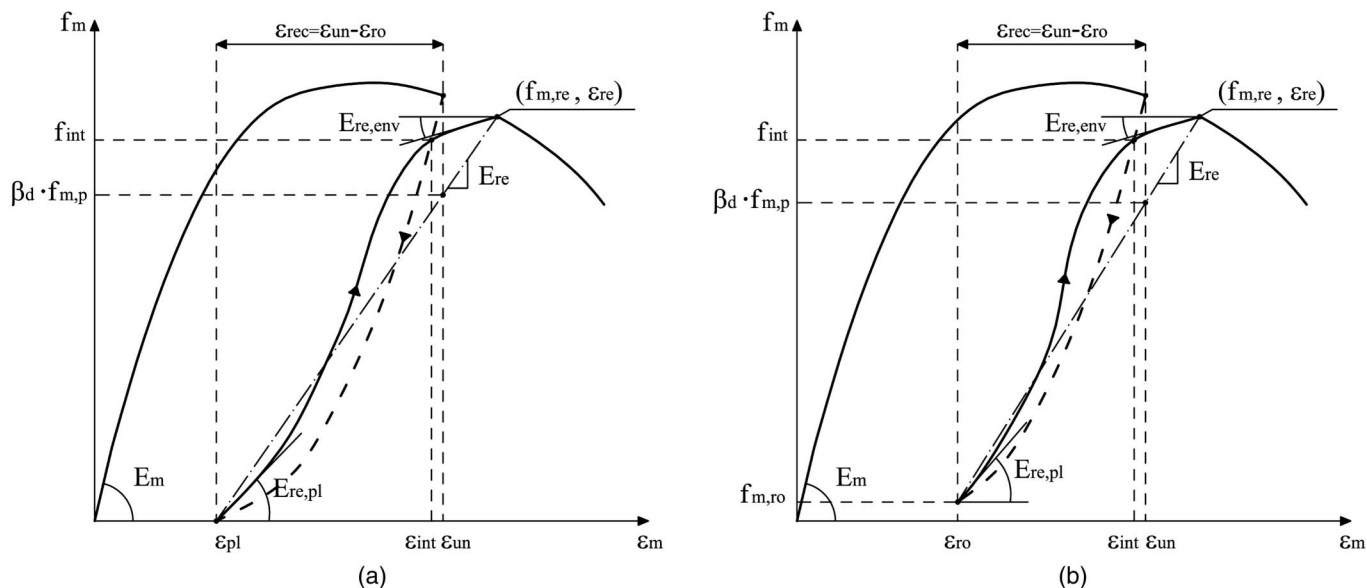


**Fig. 9.** Typical stress-strain reloading curves: (a) full unloading-reloading; (b) full reloading from partial unloading

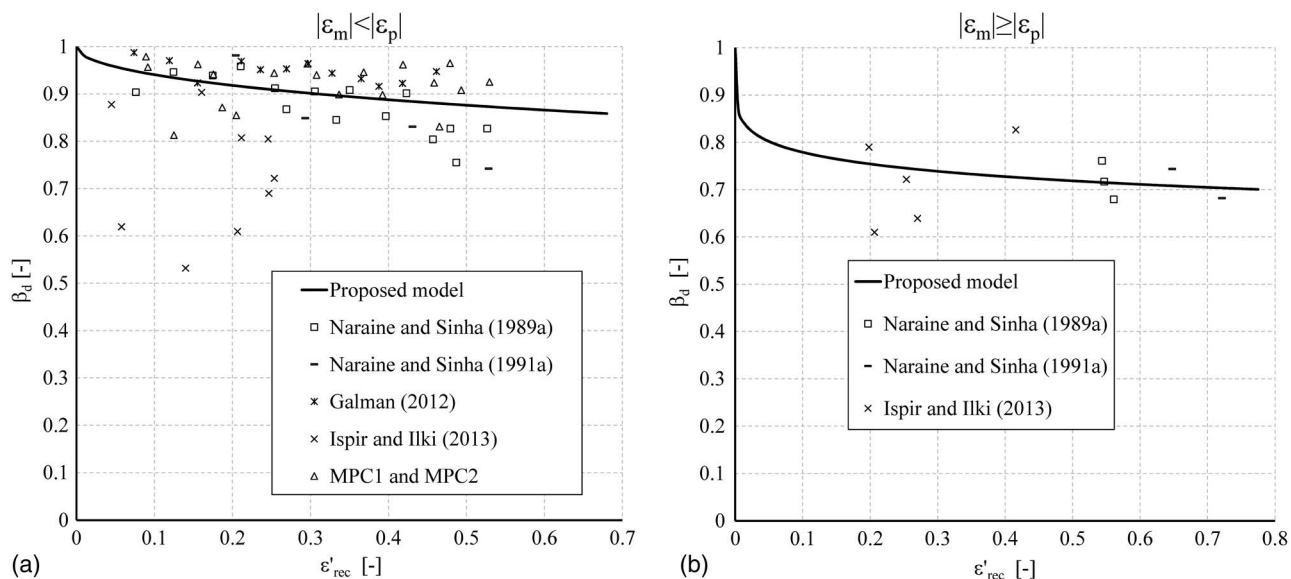


**Fig. 10.** Damage factor for masonry in compression: (a) prepeak stage; (b) postpeak stage

About the prepeak compressive behavior [Fig. 10(a)], the analytical model shows a reasonably good correlation with the experimental data despite the large scatter presented by some of the experimental results [e.g., see data from Ispir and Ilki (2013)]. Because of the lower amount of experimental data and their larger scatter, the model related to the postpeak stage [Fig. 10(b)] exhibits a poorer correlation and consequently lower accuracy in predicting the damage level of masonry. Hopefully the model will be further improved as new data become available.

The linear representation of the reloading branch adopted by other models reported in the literature is reasonable but not so accurate compared with the actual cyclic response of masonry. To better capture the actual response, a more refined nonlinear curve with double curvature should be implemented. Again, the Crisafulli's model has been used and conveniently modified by including the following boundary conditions in Eq. (3):

1. if  $\varepsilon_m = \varepsilon_{pl}$  then  $f_m = 0$ ;
2. if  $\varepsilon_m = \varepsilon_{pl}$  then  $E_1 = E_{re,pl}$ ;

3. if  $\varepsilon_m = \varepsilon_{re}$  then  $f_m = f_{m,re}$  with  $(f_{m,re}, \varepsilon_{re}) = \begin{cases} \text{Eq. (3)} \\ E_{re} \cdot (\varepsilon_m - \varepsilon_{ro}) + f_{ro} \end{cases}$ ;

4. if  $\varepsilon_m = \varepsilon_{re}$  then  $E_2 = E_{re,env}$ , where the final reloading tangent modulus  $E_{re,env}$  (Fig. 9) is provided by the following equation:

$$E_{re,env} = \max(0.5 \cdot E_{re}; \partial f_m / \partial \varepsilon_m |_{\varepsilon_m = \varepsilon_{re}}) \leq E_s \quad \text{for } \varepsilon_{re} \leq \varepsilon_p$$

$$E_{re,env} = 0.5 \cdot E_{re} \leq E_s \quad \text{for } \varepsilon_{re} > \varepsilon_p \quad (10)$$

where  $f_m$  = stress on the envelope curve according to Eq. (1). Regarding the initial reloading tangent modulus  $E_{re,pl}$ , two values are proposed depending on the unloading condition. In the case of full unloading-reloading [Fig. 9(a)], the value of  $E_{re,pl}$  can be simply estimated as follows:

$$E_{re,pl} = \gamma_{re,pl} \cdot E_{un,pl} \leq E_s \quad (11)$$

On the contrary, in the case of full reloading from partial unloading [Fig. 9(b)], the modulus  $E_{re,pl}$  is given by the following relation:

$$E_{re,pl} = \gamma_{re,pl} E_s \cdot \frac{(B_1 + 2\chi_{ro}) \cdot (1 + B_2\chi_{ro} + B_3\chi_{ro}^2) - \chi_{ro} \cdot (B_1 + \chi_{ro}) \cdot (B_2 + 2B_3\chi_{ro})}{(1 + B_2\chi_{ro} + B_3\chi_{ro}^2)^2} \leq E_s \quad (12)$$

in which  $B_1$ ,  $B_2$ ,  $B_3$ , and  $E_s$  are the same coefficients calculated for the unloading branch [Eq. (4)], whereas  $\chi_{ro} = (\varepsilon_{ro} - \varepsilon_{pl}) / (\varepsilon_{un} - \varepsilon_{pl})$ . The suggested value of the coefficient  $\gamma_{re,pl} = 1.3$  has been obtained from best fitting of experimental data.

The reloading branch is still governed by Eqs. (3) and (4), by assuming the moduli  $E_{re,pl}$ ,  $E_{re,env}$ , and  $E_{re}$  in place of  $E_1$ ,  $E_2$ , and  $E_s$ , respectively.

### Reloading Stiffness

The reloading stiffness  $E_{re}$  considers the progressive damage of masonry due to cyclic loading. Tests performed on concrete (Karsan and Jirsa 1969; Hsu 1981) and masonry (Naraine and Sinha 1989a) specimens demonstrated that the cyclic compression stress-strain curves have a locus of common points resulting from the intersection between the unloading and the reloading branch. When stresses above the common points are applied, additional strains are experienced by the specimen. On the contrary, if the specimen is repeatedly reloaded and unloaded after having achieved the common point, the reloading stiffness reduces until the hysteresis cycles go into a loop and no degradation is then observed. The common points formed by the stable loops are referred to as stability points. In the proposed model, the stress and the strain corresponding to the common point are respectively named as  $f_{int}$  and  $\varepsilon_{int}$  (Fig. 9). In cases where the stress  $f_{int}$  goes below the stability curve, that is, the locus of the stability points, the reloading stiffness ( $E_{re}$ ) must be incremented and adjusted until  $f_{int}$  equals the stability stress  $f_{stab}$ . Naraine and Sinha (1991b) and AlShebani and Sinha (1999) performed tests for estimating the value of the stability stress for masonry loaded parallel and perpendicularly to bed joints. Based on those results, a unique model has been calibrated to get a more general equation for the stability curve, independent of the loading direction. The proposed relationship has been obtained by rearranging the Smith and Young (1955) law for concrete under monotonic loading. The resulting equation in normalized form can be defined as

$$\frac{f_{stab}}{f_{m,p}} = 1.03 \cdot \varepsilon'_m \cdot e^{(1-\varepsilon'_m/0.61)} \quad \text{with } f_{stab} \leq f_{int} \quad (13)$$

A comparison between the proposed model and experimental data reported by literature is reported in Fig. 11. Considering the quite high value of the coefficient of determination ( $R^2 = 0.88$ ), Eq. (13) appears to be able to provide a good fitting of experimental data.

Eq. (13) can be applied to masonry irrespective of the direction of compressive stresses with respect to bed joints. The model assumes that the stiffness degradation occurs only if the strain achieved by the reloading path exceeds the strain  $\varepsilon_{int}$ .

### Partial Unloading/Reloading

The literature provides few experimental data regarding the cyclic compressive behavior of masonry when partial unloading/reloading occurs. On the contrary, some authors proposed models for concrete that consider the partial loadings from the full unloading/reloading curves or the case of partial unloading followed by partial reloading to strains higher than the previous maximum unloading strain. Here, the model suggested by Palermo and Vecchio (2003) for concrete has been used and adapted to represent the partial unloading/reloading response of masonry. This assumption

represents a proposal that should be validated once experimental data about partial unloading/reloading of masonry specimens subjected to axial compression will be available in literature.

As shown in Fig. 12, the partial unloading/reloading path follows different rules depending on the values of the partial unloading stress and strain ( $f_{m,un}^*$ ,  $\varepsilon_{un}^*$ ) that characterize each small cycle.

If  $\varepsilon_{un}^* \geq \varepsilon_{int}$ , material damage accumulated in the partial unloading/reloading loop is completely neglected and, therefore, the material behavior can be represented with the curves depicted in Fig. 12(a). Five branches are required to completely define the depicted model. Curve A represents the full unloading starting from the unloading strain ( $\varepsilon_{un}$ ) to the plastic offset ( $\varepsilon_{pl}$ ), and is evaluated from Eqs. (3)–(5). The unloading curve is followed by curve B described by Eq. (3) combined with Eqs. (6)–(11). If unloading takes place from a strain lower than the previous maximum strain ( $\varepsilon_{un}^*$ ), then curve C is obtained. The latter is represented by the aforementioned relations for full unloading except for the values of the unloading stress and strains that have to be updated by considering the corresponding values for the current hysteretic loop. Curve D, used here to represent the response in the case of reloading from partial unloading, results from the same relationships governing curve B, except for the initial ( $f_{m,ro}^*$ ,  $\varepsilon_{ro}^*$ ) and final ( $f_{m,un}^*$ ,  $\varepsilon_{un}^*$ ) stress-strain values. Once curve D reaches the previous unloading point ( $f_{m,un}^*$ ,  $\varepsilon_{un}^*$ ) and the strains are increased to values higher than  $\varepsilon_{un}^*$ , curve E is considered. This curve follows the same path of the reloading branch B defined after first unloading (curve A). Therefore, it is assumed that damage experienced by masonry during the first unloading phase is completely retained.

If  $\varepsilon_{un}^* < \varepsilon_{int}$ , material damage due to repeated unloading and reloading is taken into account by the model. As shown in Fig. 12(b), the procedure adopted to determine branches A, B, and C is the same as previously discussed for the case  $\varepsilon_{un}^* < \varepsilon_{int}$ . Again, the partial reloading curve D is evaluated by the equations governing full reloading but, on the contrary, coefficient  $\beta$  used to determine the

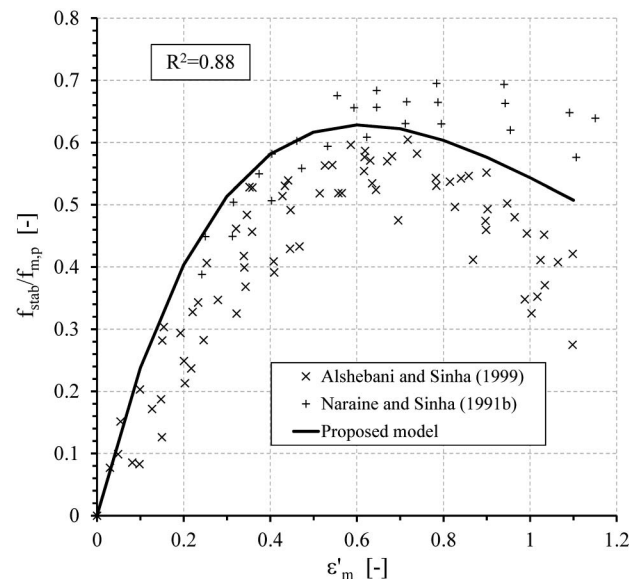


Fig. 11. Normalized stress-strain curve for determining stability point

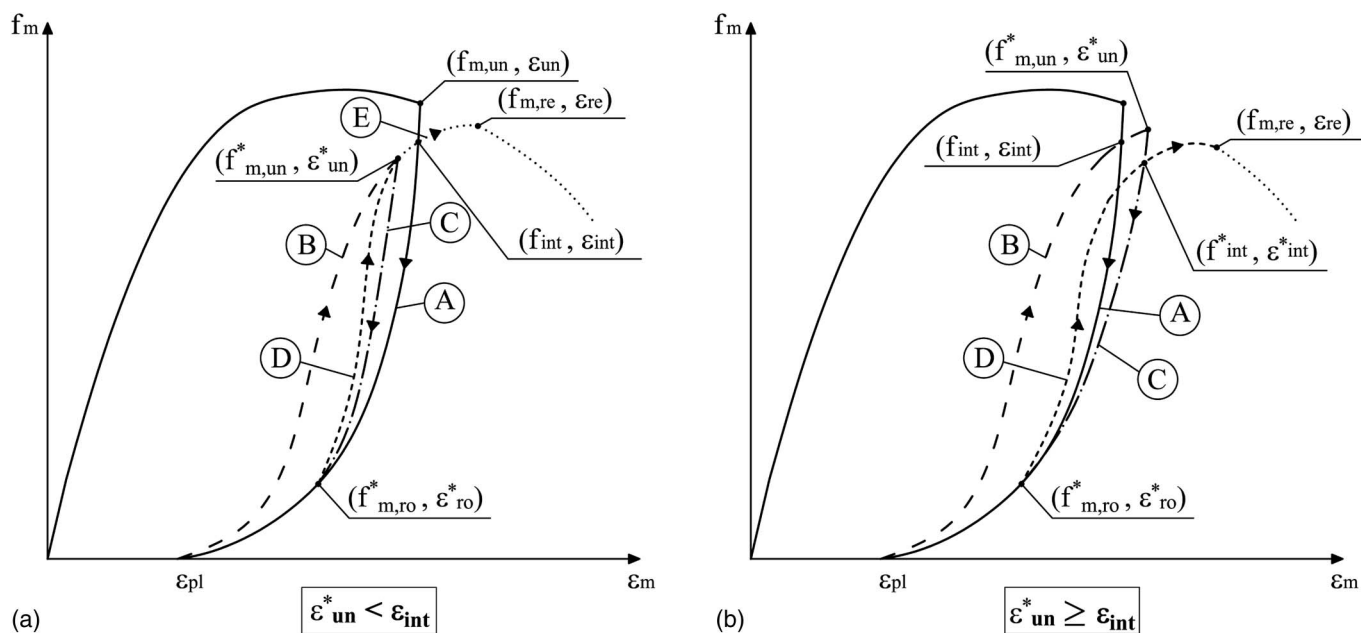


Fig. 12. Partial unloading/reloading model for (a)  $\varepsilon_{un}^* < \varepsilon_{int}$ ; (b)  $\varepsilon_{un}^* \geq \varepsilon_{int}$

reloading stiffness  $E_{re}$  and the related reloading stress  $f_{re}$  and strain  $\varepsilon_{re}$  on the envelope curve is calculated [see Eqs. (8) and (9)] assuming  $\varepsilon'_{rec} = (\varepsilon_{un}^* - \varepsilon_{ro}^*) / \varepsilon_p$ . Further partial unloading/reloading cycles starting from new values of the unloading strains  $\varepsilon_{un}^*$  lower than  $\varepsilon_{re}$  will be obtained according to the previous procedure after having updated the values of the intersection strain ( $\varepsilon_{int} = \varepsilon_{int}^*$ ) and stress ( $f_{int} = f_{int}^*$ ).

One should observe that the residual plastic strain  $\varepsilon_{pl}$  is always considered constant unless the compressive strain  $\varepsilon_m$  exceeds the reloading strain  $\varepsilon_{re}$  on the envelope curve.

## Model Verification

The proposed model is used to predict the response of some experimental tests involving solid brick masonry panels subjected to uniaxial compressive cyclic loading. In more detail, the analytical procedure previously discussed has been implemented in a finite element program (Wong et al. 2013), which has been used to predict the response of each test.

As shown in Fig. 13, the simulations included the experimental tests carried out by Naraine and Sinha (1989b), Galman (2012), and Oliveira (2003), as well as specimen MPC2 tested in this research. All the predictions assumed the strains at the onset of the unloading curves as the reverse point for the analytical model. Moreover, the same parameters of the envelope curves reported in Table 1 were used as input data for the proposed model. Table 2 compares the energy density dissipated within each cycle by the test specimens ( $E_{exp}$ ) with that ( $E_{an}$ ) resulting from the analytical simulation. The relative error reported in the table is evaluated as  $Err = (E_{an} - E_{exp}) \cdot 100 / E_{exp}$ .

The simulation of the test performed by Naraine and Sinha (1989b), on a specimen loaded perpendicularly to bed joints, provides a good prediction of the actual experimental response [Fig. 13(a)]. The adopted value of the initial unloading modulus  $E_{un}$  seems to properly fit the initial slope of the experimental unloading curves. The model proposed for estimating plastic strains provides strain values quite close to the real ones. As shown in Fig. 13(a) and confirmed by data reported in Table 2, the shape

of the unloading and reloading curves causes an overestimation of the dissipated energy ranging from 5 to 63%. In spite of this, the overall approximation of the experimental response is satisfactory.

Unlike the previous case study, the experimental test carried out by Galman (2012) is limited to the prepeak behavior of the material. The analytical prediction [Fig. 13(b)] is quite accurate and, except for the first loading cycle, the relative error related to the prediction of the dissipated energy ranged from  $-4$  to  $+37\%$  (Table 2).

The test performed by Oliveira (2003) [Fig. 13(c)] is the only example here available including loops characterized by reloading after partial unloading from the envelope curve. All the predicted unloading and reloading branches seem to be consistent with the experimental ones in spite of the not excellent estimation of the stress corresponding to the strain at the onset of reloading of the second and third cycle. The predicted and the experimental dissipated energy is found to be very similar (Table 2).

The cyclic curves resulting from the simulation of the specimens MPC1 and MPC2 are depicted in Figs. 13(d and e). In spite of the not excellent estimation of the response at the onset of unloading, the value of the coefficient  $\gamma_{un}$  has been kept equal to the default value 1.5. Note that the latter is equal to the maximum value suggested by Crisafulli (1997) to get a realistic representation of the masonry behavior at unloading. Because of the better prediction of the plastic offset strain, the unloading curves exhibited by the specimen MPC2 [Fig. 13(e)] resulted to be more consistent with the experimental response than those observed for the Specimen MPC1 [Fig. 13(e)]. The reloading curves related to the Specimen MPC1 appeared to be quite consistent with the corresponding experimental response. On the contrary, the inability of the envelope curve to simulate the considerable stiffness degradation presented by the specimen MPC2 led to a not good estimation of the reloading response. As expected, compared with the experimental response, the predicted dissipated energy related to the specimen MPC1 was underestimated (i.e., Err ranged from  $-44$  to  $-6\%$ ) whereas the energy dissipated by the specimen MPC2 was overestimated (i.e., Err ranged from  $+15$  to  $+55\%$ ) (Table 2).

All the predictions have in common the same drawback regarding the determination of the intersection between the reloading

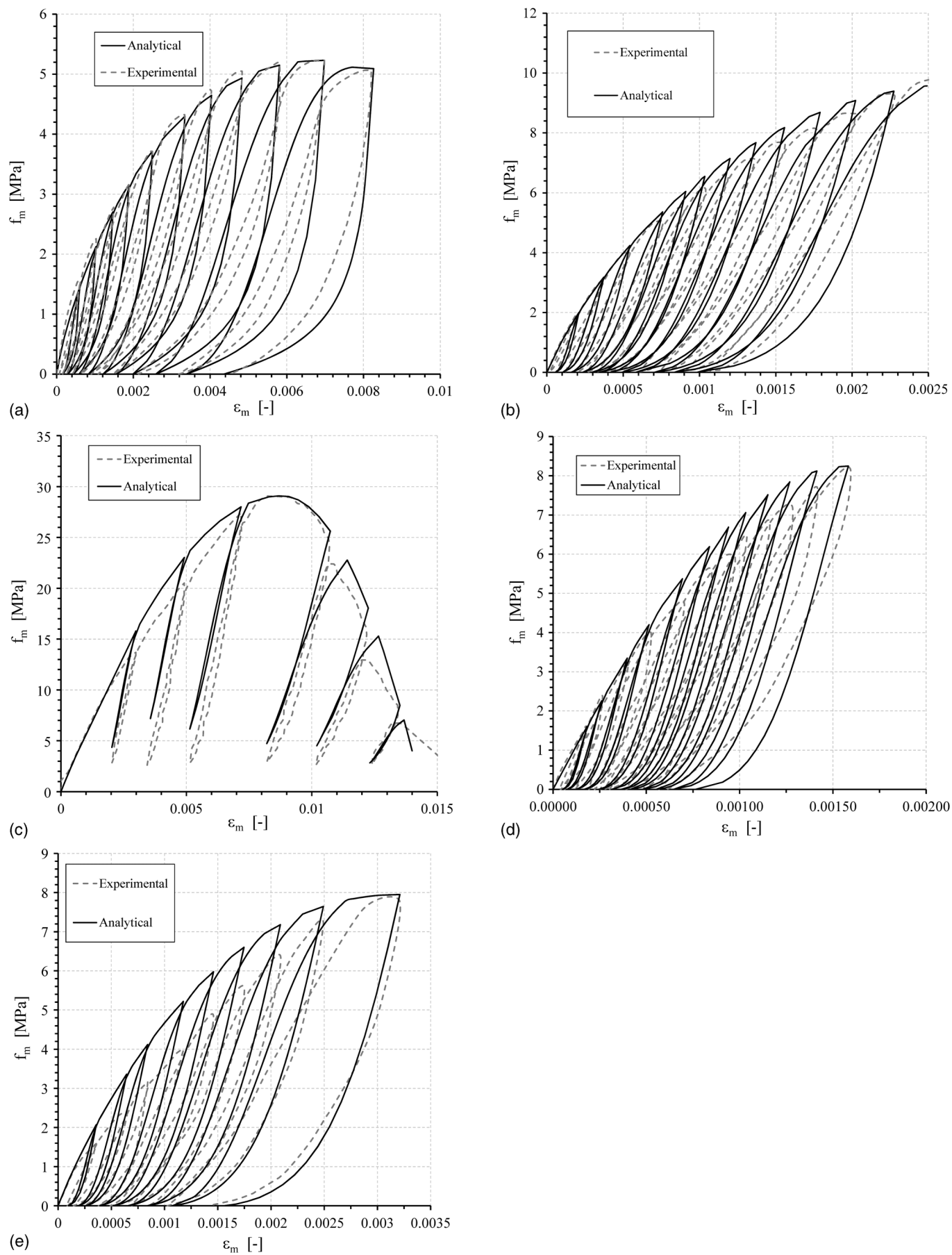


**Fig. 13.** Simulation of cyclic compression tests by the proposed model: (a) Naraine and Sinha (1989b); (b) Galman (2012); (c) Oliveira (2003); (d) specimen MPC1; (e) specimen MPC2

**Table 2.** Experimental versus Analytical Evaluation of the Dissipated Energy Density

Specimen	Property	Unit	Cycle												
			1	2	3	4	5	6	7	8	9	10	11	12	13
Naraine and Sinha (1989b)	$E_{exp}$	kN/m <sup>2</sup>	0.27	0.53	0.66	0.99	1.8	2.7	2.5	3.9	6	6.9	7.4	—	—
	$E_{an}$		0.28	0.58	0.97	1.3	2.2	3.7	4.1	5.3	6.9	9.3	10	—	—
	Eirr	%	+5	+9	+47	+32	+27	+35	+63	+34	+14	+34	+41	—	—
Galman (2012)	$E_{exp}$	kN/m <sup>2</sup>	0.07	0.22	0.41	0.73	0.70	0.81	0.99	1.30	1.60	1.90	2.40	2.6	7.1
	$E_{an}$		0.13	0.30	0.53	0.93	0.81	0.81	1.10	1.40	1.60	2.20	2.40	2.9	6.8
	Eirr	%	+72	+23	+18	+18	+37	+22	+37	+25	+21	+32	+17	+27	-4
Oliveira (2003)	$E_{exp}$	kN/m <sup>2</sup>	16.0	28.0	46.0	100	46.0	26.0	6.2	—	—	—	—	—	—
	$E_{an}$		14.0	27.0	45.0	100	43.0	30.0	7.0	—	—	—	—	—	—
	Eirr	%	-11	-2	-2	0	-5	+18	+14	—	—	—	—	—	—
MPC1	$E_{exp}$	kN/m <sup>2</sup>	0.09	0.13	0.28	0.47	0.72	0.92	1.06	1.03	1.29	1.36	1.32	2.0	—
	$E_{an}$		0.07	0.08	0.22	0.28	0.58	0.66	0.59	0.63	0.83	0.94	1.24	1.6	—
	Eirr	%	-17	-34	-21	-40	-20	-29	-44	-39	-35	-30	-6	-23	—
MPC2	$E_{exp}$	kN/m <sup>2</sup>	0.18	0.44	0.59	0.82	1.18	1.56	2.02	2.54	5.18	—	—	—	—
	$E_{an}$		0.21	0.50	0.59	1.27	1.50	1.87	2.54	3.37	6.21	—	—	—	—
	Eirr	%	+18	+15	0	+55	+28	+20	+26	+33	+20	—	—	—	—

and the unloading path, often referred to as the common point. More specifically, the common point is generally overestimated in the prepeak stage and underestimated in the postpeak response. However, considering the overall good quality of the predictions obtained, the aforementioned drawback appears not to be of primary importance.

Finally, the intersection of the reloading branch with the envelope curve is not always well approximated in the performed simulations. This fact is directly related to the adopted envelope model that does not perfectly fit the experimental curves (Fig. 6).

An additional simulation has been performed to assess the ability of the model to predict the progressive stiffness degradation resulting from repeated cycles of full unloading and reloading at maximum strain not lower than the intersection strain  $\varepsilon_{int}$ . The experimental test performed by AlShebani and Sinha (1999) to determine the stability points has been used here as a reference example [Fig. 14(a)]. The parameters used to define the envelope curve are reported in Fig. 14(a). To better highlight the prediction results, the comparison of the analytical response with the experimental curve has been limited to strains ranging between 0.004 and 0.0092. As shown in Fig. 14(b), the actual unloading paths are not well captured by the proposed model that tends to considerably underestimate the unloading stiffness. This fact is mainly due to the slope of the actual curve at the onset of unloading, whose value is unusually negative, contrary to the assumptions of the proposed model [Eq. (5)]. Despite this deficiency, the analytical model provides a reasonable simulation of the repeated partial unloading/reloading cycles and gives a good prediction of the stability stress value.

## Conclusions

This paper presents a new constitutive model for simulating the compressive behavior of brick masonry subjected to cyclic loading. The relationships implemented have been formulated in terms of average stresses and strains consistent with the typical analysis approaches based on the smeared crack concept. To represent unloading and reloading, the nonlinear curves included in the model proposed by Crisafulli (1997) have been modified in order to obtain a more generalized model suitable for different brick masonry typologies. The novel features introduced herein can be summarized as follows:

1. An empirical model depending on the normalized strain at the onset of unloading is proposed for predicting the instantaneous value of residual plastic strain. The formulation has been calibrated by nonlinear regression analysis of several data collected from the literature concerning compression cyclic tests on different types of brick masonry specimens.
2. The unloading response has been modeled by a nonlinear relationship, starting from the envelope curve, whose shape can be controlled by changing the initial and final tangent moduli. The latter can be estimated by simple relationships specifically calibrated from regression of experimental data provided in the literature.
3. To provide an accurate representation of the reloading response, a double-curvature law has been implemented. Unlike similar models, the reloading curve depends on a reloading stiffness parameter that, in turn, results from a degrading function that is able to account for the progressive damage of masonry due to cyclic loading. A linear relationship having a slope equal to the reloading stiffness has been used to determine the point of intersection between the reloading and the envelope curve. All

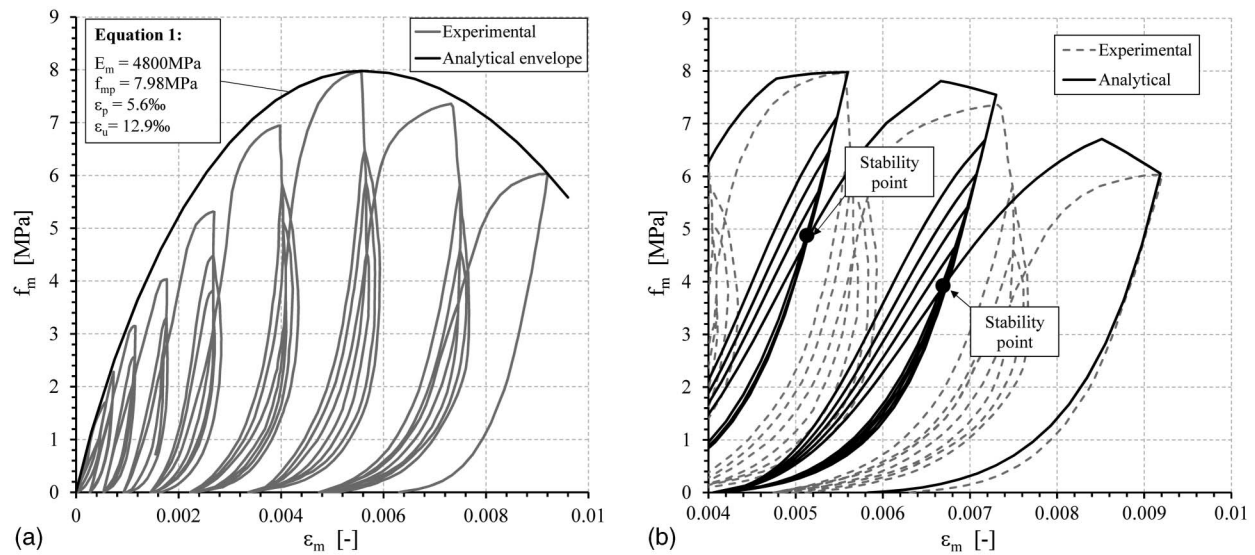


**Fig. 14.** Experimental test performed by Alshebani and Sinha (1999): (a) overall experimental response; (b) simulation of the last hysteresis loops by the proposed analytical model

the parameters included in the formulations have been experimentally calibrated.

- A model for considering partial unloading and reloading has been also proposed and implemented.

The ability of the model to predict the cyclic compressive response of brick masonry has been established by simulating different experimental tests on masonry panels. All the simulations agreed reasonably well with the experimental results.

## Acknowledgments

The authors would like to thank engineer Marta Vacchelli for her contribution in performing tests and postprocessing data. The support provided by the laboratory technicians Andrea Delbarba and Luca Martinelli is also strongly acknowledged.

## Notation

The following symbols are used in this paper:

- $E_{an}$  = analytical energy density dissipated within each cycle;
- $E_{exp}$  = experimental energy density dissipated within each cycle;
- $E_m$  = initial elastic tangent modulus;
- $E_{re}$  = reloading stiffness;
- $E_{re,env}$  = final tangent stiffness of the reloading curve;
- $E_{re,pl}$  = initial tangent stiffness of the reloading curve;
- $E_s f_{m,un} / (\varepsilon_{un} - \varepsilon_{pl})$  = secant modulus referred to the unloading branch;
- $E_{sec} = f_{m,p} / |\varepsilon_p|$  = secant modulus referred to the envelope curve;
- $E_{un}$  = initial tangent stiffness of the unloading curve;
- $E_{un,pl}$  = stiffness at zero stress after total unloading;
- $f_m$  = compressive stress of masonry;
- $f'_m$  = normalized compressive stress of masonry;
- $f_{m,int}$  = stress at the intersection between the unloading and reloading branch (common point);
- $f_{m,int}^*$  = stress at the intersection between the partial unloading and reloading branch;

- $f_{m,p}$  = stress at peak of the envelope curve;
- $f_{m,re}$  = stress at the intersection between the reloading and the envelope curve;
- $f_{m,ro}$  = stress at onset of reloading;
- $f_{m,ro}^*$  = stress at onset of partial reloading;
- $f_{m,un}$  = stress at onset of unloading;
- $f_{m,un}^*$  = stress at onset of partial unloading;
- $f_{stab}$  = stress on the stability curve;
- $\beta_d$  = damage factor;
- $\varepsilon_{int}$  = strain at the intersection between the unloading and reloading branch (common point);
- $\varepsilon_{int}^*$  = strain at the intersection between the partial unloading and reloading branch;
- $\varepsilon_m$  = compressive strain of masonry;
- $\varepsilon'_m$  = normalized strain of masonry;
- $\varepsilon_p$  = strain at peak of the envelope curve;
- $\varepsilon'_p$  = normalized value of the strain at peak of each cycle;
- $\varepsilon_{pl}$  = plastic offset strain;
- $\varepsilon'_{pl}$  = normalized plastic offset strain;
- $\varepsilon_{re}$  = strain at the intersection between the reloading and the envelope curve;
- $\varepsilon'_{rec}$  = normalized recovery strain;
- $\varepsilon_{ro}$  = strain at onset of reloading;
- $\varepsilon_{ro}^*$  = strain at onset of partial reloading;
- $\varepsilon_u$  = ultimate strain of masonry;
- $\varepsilon_{un}$  = unloading strain;
- $\varepsilon'_{un}$  = normalized unloading strain at the intersection between the envelope and the loading/reloading curve; and
- $\varepsilon_{un}^*$  = strain at onset of partial unloading.

## References

- AlShebani, M. M. (2001). "Cyclic residual strains of brick masonry." *Proc., Int. Conf. on Structural Engineering, Mechanics, and Computation*, A. Zingoni, ed., Vol. 1, Elsevier, Amsterdam, Netherlands, 437–445.
- AlShebani, M. M., and Sinha, N. (1999). "Stress-strain characteristics of brick masonry under uniaxial cyclic loading. Behavior of brick masonry

- under cyclic compressive loading." *J. Struct. Eng.*, 10.1061/(ASCE)0733-9445(1999)125:6(600), 600–604.
- BSI (British Standards Institution). (2007). "Methods of test for mortar for masonry. 11: Determination of flexural and compressive strength of hardened mortar." *BS EN 1015-11:2007*, London.
- BSI (British Standards Institution). (2011). "Methods of tests for masonry units. 1: Determination of compressive strength." *BS EN 772-1:2011*, London.
- Chaimoon, K., and Attard, M. M. (2007). "Modeling of unreinforced masonry walls under shear and compression." *Eng. Struct.*, 29(9), 2056–2068.
- Crisafulli, F. J. (1997). "Seismic behaviour of reinforced concrete structures with masonry infills." Ph.D. thesis, Dept. of Civil Engineering, Univ. of Canterbury, Christchurch, New Zealand, 404.
- Eibl, J., Keintzel, E., and Vratsanou, V. (1996). "Determination of earthquake duration dependent behaviour factors for unreinforced brick masonry panels by nonlinear time history calculations." *Proc., 11th World Conf. on Earthquake Engineering*, Elsevier, Amsterdam, Netherlands.
- Faconi, L., Plizzari, G., and Vecchio, F. (2014). "Disturbed stress field model for unreinforced masonry." *J. Struct. Eng.*, 10.1061/(ASCE)ST.1943-541X.0000906, 04013085.
- Galman, I. (2012). "Ściany z ceramicznej cegły pełnej cyklicznie ściskane w swej płaszczyźnie lub zginane prostopadle do płaszczyzny." Ph.D. thesis, Silesian Univ. of Technology, Gliwice, Poland, 19 (in Polish).
- Gambarotta, L., and Lagomarsino, S. (1997). "Damage models for the seismic response of brick masonry shear walls. II: The continuum model and its application." *Earthquake Eng. Struct. Dyn.*, 26(4), 441–462.
- Hoshikuma, J., Kawashima, K., Nagaya, K., and Taylor, A. W. (1997). "Stress-strain model for confined reinforced concrete in bridge piers." *J. Struct. Eng.*, 10.1061/(ASCE)0733-9445(1997)123:5(624), 624–633.
- Hsu, T. C. (1981). "Fatigue of plain concrete." *J. Amer. Concr. Inst.*, 78(4), 292–305.
- Ispir, M., and Ilki, A. (2013). "Behavior of historical unreinforced brick masonry walls under monotonic and cyclic compression." *Arabian J. Sci. Eng.*, 38(8), 1993–2007.
- Karsan, I. K., and Jirsa, J. O. (1969). "Behaviour of concrete under compressive loadings." *J. Struct. Div.*, 95(12), 2543–2563.
- Lourenço, P. B., and Rots, J. G. (1997). "Multisurface interface model for analysis of masonry structures." *J. Struct. Eng.*, 10.1061/(ASCE)0733-9399(1997)123:7(660), 660–668.
- Lourenço, P. B., Rots, J. G., and Blaauwendraad, J. (1998). "Continuum model for masonry: Parameter estimation and validation." *J. Struct. Eng.*, 10.1061/(ASCE)0733-9445(1998)124:6(642), 642–652.
- Mander, J. B., Priestley, M. J. N., and Park, R. (1988). "Theoretical stress-strain model for confined concrete." *J. Struct. Eng.*, 10.1061/(ASCE)0733-9445(1988)114:8(1804), 1804–1826.
- Mehrabi, A. B., and Shing, P. B. (1997). "Finite element modeling of masonry-infilled RC frames." *J. Struct. Eng.*, 10.1061/(ASCE)0733-9445(1997)123:5(604), 604–613.
- Naraine, K., and Sinha, N. (1989a). "Behavior of brick masonry under cyclic compressive loading." *J. Struct. Eng.*, 10.1061/(ASCE)0733-9445(1989)115:6(1432), 1432–1445.
- Naraine, K., and Sinha, S. (1989b). "Loading and unloading stress-strain curves for brick masonry." *J. Struct. Eng.*, 10.1061/(ASCE)0733-9445(1989)115:10(2631), 2631–2644.
- Naraine, K., and Sinha, S. (1991a). "Cyclic behavior of brick masonry under biaxial compression." *J. Struct. Eng.*, 10.1061/(ASCE)0733-9445(1991)117:5(1336), 1336–1355.
- Naraine, K., and Sinha, S. (1991b). "Model for cyclic compressive behavior of brick masonry." *ACI Struct. J.*, 88(5), 592–602.
- Oliveira, D. V. (2003). "Experimental and numerical analysis of blocky masonry structures under cyclic loading." Ph.D. dissertation, Universidade do Minho, Guimarães, Portugal.
- Palermo, D., and Vecchio, F. J. (2003). "Compression field modeling of reinforced concrete subjected to reversed loading: Formulation." *ACI Struct. J.*, 100(5), 616–625.
- Papa, E. (2001). "Damage and failure models." *Computational modelling of masonry brickwork and blockwork structures*, Saxe-Coburg Publications, Stirling, Scotland, 1–26.
- Rots, J. G. (1988). "Computational modeling of concrete fracture." Ph.D. thesis, Delft Univ. of Technology, Delft, Netherlands.
- Seckin, M. (1981). "Hysteretic behaviour of cast-in-place exterior beam-column sub-assemblies." Ph. D. thesis, Univ. of Toronto, Toronto, 266.
- Sima, J. F., Roca, P., and Molins, C. (2011). "Nonlinear response of masonry wall structures subjected to cyclic and dynamic loading." *Eng. Struct.*, 33(6), 1955–1965.
- Smith, G. M., and Young, L. E. (1955). "Ultimate theory in flexure by exponential function." *J. Am. Concr. Inst.*, 52(3), 349–359.
- Subramaniam, K. V. L., and Sinha, S. N. (1995). "Analytical model for cyclic compressive behavior of brick masonry." *ACI Struct. J.*, 92(3), 288–294.
- Vecchio, F. J. (2000). "Disturbed stress field model for reinforced concrete: Formulation." *J. Struct. Eng.*, 10.1061/(ASCE)0733-9445(2000)126:9(1070), 1070–1077.
- Wong, P. S., Vecchio, F. J., and Tammels, H. (2013). "*VecTor2 & formworks user's manual*, 2nd Ed., Dept. of Civil Engineering, Univ. of Toronto, Toronto, 318.